Colloids and Surfaces B: Biointerfaces 199 (2021) 111530

Contents lists available at ScienceDirect

Colloids and Surfaces B: Biointerfaces

journal homepage: www.elsevier.com/locate/colsurfb

Design and development of poly-L/D-lactide copolymer and barium titanate nanoparticle 3D composite scaffolds using breath figure method for tissue engineering applications

H. Kemppi [a,*], M.A. Finnilä [a], G.S. Lorite [b], M. Nelo [b], J. Juuti [b], M. Kokki [c], H. Kokki [d], J. Räsänen [e], A. Mobasheri [a,f,g], S. Saarakkala [a,h]

[a] Research Unit of Medical Imaging, Physics and Technology, Faculty of Medicine, University of Oulu, Oulu, FI-90220, Finland
[b] Microelectronics Research Unit, Faculty of Information Technology and Electrical Engineering, University of Oulu, Oulu, FI-90570, Finland
[c] Department of Anaesthesia and Intensive Care, Kuopio University Hospital, Kuopio, FI-7002, Finland
[d] School of Medicine, University of Eastern Finland, Kuopio, FI-70210, Finland
[e] Department of Obstetrics and Gynecology, Helsinki University Hospital and University of Helsinki, Helsinki, FI- 00099, Finland
[f] Department of Regenerative Medicine, State Research Institute Centre for Innovative Medicine, Vilnius, LT-08406, Lithuania
[g] University Medical Center Utrecht, Department of Orthopedics, Rheumatology and Clinical Immunology, Utrecht, 508 GA, the Netherlands
[h] Department of Diagnostic Radiology, Oulu University Hospital, Oulu, FI-90220, Finland

ARTICLE INFO

Keywords:
3D composite scaffold
Poly-L/D-lactide copolymer
Barium titanate nanoparticle
Breath figure method
Tissue engineering

ABSTRACT

In tissue engineering, the scaffold topography influences the adhesion, proliferation, and function of cells. Specifically, the interconnected porosity is crucial for cell migration and nutrient delivery in 3D scaffolds. The objective of this study was to develop a 3D porous composite scaffold for musculoskeletal tissue engineering applications by incorporating barium titanate nanoparticles (BTNPs) into a poly-L/D-lactide copolymer (PLDLA) scaffold using the breath figure method. The porous scaffold fabrication utilised 96/04 PLDLA, dioleoyl phosphatidylethanolamine (DOPE), and different types of BTNPs, including uncoated BTNPs, Al_2O_3-coated BTNPs, and SiO_2-coated BTNPs. The BTNPs were incorporated into the polymer scaffold, which was subsequently analysed using field emission scanning electron microscopy (FE-SEM). The biocompatibility of each scaffold was tested using ovine bone marrow stromal stem cells. The cell morphology, viability, and proliferation were evaluated using FE-SEM, LIVE/DEAD staining, and Prestoblue assay. Porous 3D composite scaffolds were successfully produced, and it was observed that the incorporation of uncoated BTNPs increased the average pore size from 1.6 μm (PLDLA) to 16.2 μm (PLDLA/BTNP). The increased pore size in the PLDLA/BTNP scaffolds provided a suitable porosity for the cells to migrate inside the scaffold, while in the pure PLDLA scaffolds with their much smaller pore size, cells elongated on the surface. To conclude, the breath figure method was successfully used to develop a PLDLA/BTNP scaffold. The use of uncoated BTNPs resulted in a composite scaffold with an optimal pore size while maintaining the honeycomb-like structure. The composite scaffolds were biocompatible and yielded promising structures for future tissue engineering applications.

1. Introduction

Tissue engineering is an interdisciplinary field of research and development that combines scaffolds, cells, and biologically active molecules into functional tissues. It is a promising method to repair damaged tissues [1,2]. The topography of the scaffold, including its roughness, porosity, and other surface features, influence cell adhesion, proliferation, and function [3,4]. Scaffolds should mimic the natural extracellular matrix (ECM). Furthermore, interconnected porosity is a crucial feature for cell attachment, cell migration, nutrient delivery, and matrix production for tissue engineering scaffolds [5]. Porous scaffolds can be produced using various methods such as photolithography, soft lithography, colloidal lithography, electron beam lithography, polymer phase separation, and chemical vapour deposition [6–8]. Likewise, the breath figure method can be used to develop 3D porous scaffolds with patterned pore structures [9–11]. This processing method provides a

* Corresponding author.
E-mail address: hanna.kemppi@oulu.fi (H. Kemppi).

https://doi.org/10.1016/j.colsurfb.2020.111530
Received 25 September 2020; Received in revised form 30 November 2020; Accepted 7 December 2020
Available online 13 December 2020

simple and low-cost approach to produce scaffolds with varying pore structures. In the breath figure method, a polymer is dissolved in a volatile solvent and cast under high humidity. During the evaporation of the solvent, water droplets in the humid air condense onto the polymer solution and form a honeycomb-patterned pore structure on the scaffold. These kinds of honeycomb scaffolds are suitable for the 3D culturing of various cell types, such as mesenchymal stem cells [12,13], adipose-derived stem cells [14], osteoblasts [15] and chondrocytes [16, 17].

Concerning the materials used in scaffolds, polylactic acid (PLA) has been approved by the Food and Drug Administration (FDA) for clinical use and is widely used in medical applications because of its good biocompatibility, suitable degradation rate, and potential for use with various processing methods [18]. Using PLA and dioleoylphosphatidylethanolamine (DOPE) as a surfactant, porous scaffolds have previously been produced using the breath figure method [14,16, 19–21]. DOPE has been used as a surfactant to stabilise the water droplets on the polymer surface, which leads to the formation of a honeycomb structure in PLA scaffolds [20].

In most tissue engineering applications, one material alone cannot be used to create a functional scaffold [22]. When multiple materials are incorporated into a scaffold, composite structures can be created. This allows the tuning of the topographical and mechanical characteristics, as well as the addition of new functionalities for the scaffold. Nanoparticles are fascinating choices because they have a large surface-to-volume ratio and can be tailored for specific physical properties, including optical, magnetic, electrical, and piezoelectrical properties [23,24]. Barium titanate ($BaTiO_3$) is a ferroelectric ceramic with a high dielectric constant and relatively high piezoelectricity. Moreover, barium titanate nanoparticles (BTNPs) are also non-toxic at high concentrations [25]. By adding a piezoelectric material to the composite, electrically active scaffolds have previously been proposed [26]. Piezoelectric nanoparticles can provide electromechanical stimulation to the cells, which can beneficially modify cellular behaviours [27].

In this work, PLDLA and BTNPs with different inorganic coatings were used to develop 3D composite scaffolds using the breath figure method. Finally, an *in vitro* biocompatibility assessment of the cell viability, morphology, and proliferation was conducted for the most promising 3D composite scaffold for tissue engineering applications using ovine bone marrow stromal stem cells.

2. Materials and methods

2.1. Scaffold preparation and material characterisation

2.1.1. BTNP characterisation

Three different types of BTNPs (provided by Sachtleben Pigments Oy, Finland) were studied: uncoated (BTNP), Al_2O_3-coated (BTNP-Al_2O_3), and SiO_2-coated (BTNP-SiO_2). The elemental composition and size of the nanoparticles were characterised using scanning transmission electron microscopy (STEM) device (JEOL JEM-2200FS, Japan), equipped with an energy-dispersive detector (EDS). A small quantity of nanoparticles was suspended in 70 % ethanol, pipetted onto a carbon film (Lacey, LC200-CU-100, Electron Microscopy Science, USA), and left to dry at room temperature. The size distribution of the nanoparticles was measured (>100 measurements for each nanoparticle type) from the STEM images using the EM software Beta 0.85 (Teitz Video and Image Processing Systems GmbH).

2.1.2. Scaffold preparation

Copolymer 96/04 L-lactide-D-lactide copolymer (PLDLA, PURASORB® PLD 9620, Corbion Purac, Netherlands) and dioleoyl phosphatidylethanolamine (DOPE, Sigma, Japan) were used to produce porous 3D scaffolds using the breath figure method as previously described [19]. PLDLA and DOPE were dissolved in chloroform at concentrations of 10 mg/mL and 0.1 mg/mL, respectively. For the composite scaffold preparation, 20 wt% of nanoparticles were dissolved in the DOPE solution and sonicated for 10 min.

The PLDLA solution was mixed with two different DOPE solutions (with and without nanoparticles). All the scaffolds were prepared by casting 500 μL of the mixed solution onto a glass Petri dish. The chloroform was allowed to evaporate under airflow in 80 % humidity, and the scaffolds were left to dry overnight at room temperature. The next day, the scaffolds were washed three times with 70 % ethanol and left to dry at room temperature.

The scaffolds were designated as follows: a pure poly-L/D-lactide copolymer scaffold as “PLDLA”, poly-L/D-lactide copolymer and uncoated BTNP composite scaffold as “PLDLA/BTNP”, poly-L/D-lactide copolymer and aluminium oxide-coated BTNP composite scaffold as “PLDLA/BTNP-Al_2O_3”, and poly-L/D-lactide copolymer and silicon dioxide-coated BTNP composite scaffold as “PLDLA/BTNP-SiO_2”.

2.1.3. Scaffold characterisation

The structure and porosity of each scaffold, as well as its nanoparticle distribution, were evaluated using field emission scanning electron microscopy (FE-SEM) for the PLDLA and PLDLA with nanoparticles (Σigma HD VP, Carl Zeiss Microscopy GmbH, Germany and Zeiss ULTRA plus, Germany). The samples were prepared for FE-SEM by coating them with carbon. The mean pore size was manually measured (500 measurements from each scaffold type) from FE-SEM images using ImageJ software (US National Institutes of Health).

2.2. Biocompatibility of scaffolds

2.2.1. Isolation of ovine stromal stem cells

Stromal stem cells were collected from the bone marrow of the femurs of adult female åland sheep after euthanasia. The animals were part of another research project approved by the National Animal Experiment Board of Finland (ESAVI/1007/04.10.07/2014, http://www.avi.fi/web/avi/elainkoelautakunta-ella). The animal transport, housing, care, and experimental procedures were conducted according to the national legislation [28] and EU Directive 2010/63/EU [29].

The bone marrow aspirates were transferred into minimum essential medium alpha (α-MEM, Corning) supplemented with 2% antibiotics (100 U mL-1 penicillin, 100 μg mL-1 streptomycin, P/S, Gibco) and 1% amphotericin B (Sigma). The suspension was centrifuged, and the supernatant was discarded. Bone marrow clots were placed into cell culture flasks and cultured in α-MEM supplemented with 10 % heat-inactivated foetal bovine serum (FBS, Biowest, South America) and 1% P/S at 37 °C and 5% CO_2. After 48 h, the flasks were washed with phosphate buffered saline (PBS, Gibco) three times to remove the non-adherent cells and bone marrow clots. The cells were cultured until confluence, and the medium was changed three times per week.

2.2.2. Seeding ovine stromal stem cells

The scaffolds were sterilised by dipping them into 70 % ethanol for 15 min. They were washed three times with PBS and left in the cell culture medium before cell seeding. Ovine bone marrow stromal stem cells at passage 2 were seeded at a density of 20,000 cells/cm^2 on top of the scaffolds. The cells were cultured for 2 weeks, and the medium was changed three times per week.

2.2.3. Cell attachment and morphology

The cell attachment and morphology were studied after 7 and 14 days using FE-SEM. The samples were washed with PBS and fixed in 2.5 % glutaraldehyde in phosphate buffer (0.1 M). Dehydration was performed in the graded ethanol series and dried using a critical dryer (K850, Quorum Technologies, UK). The samples were sputtered with a thin carbon layer (Q150 T ES, Quorum Technologies, UK) and imaged using FE-SEM (Σigma HD VP, Carl Zeiss Microscopy GmbH, Oberkochen, Germany).

2.2.4. Cell viability

The cell viability on each scaffold was analysed at days 1 and 14 with LIVE/DEAD staining (Invitrogen, Thermo Fisher Scientific, US). The scaffolds were lifted to new wells and washed once with PBS. The cells were stained for 40 min at 37 °C in a solution containing 0.5 μM calcein AM and 0.25 μM ethidium homodimer diluted in PBS. After incubation, the staining solution was replaced with PBS, and the samples were immediately imaged using a Leica SP8 FALCON laser scanning confocal microscope (Leica Microsystems GmbH, Germany). The reflection imaging mode was used to acquire 3D images.

2.2.5. Cell proliferation

The cell proliferation was quantified after 1 and 14 days with Prestoblue™ cell viability reagent (Thermo Fisher Scientific, Invitrogen, USA). The scaffolds were lifted to new wells and washed once with PBS. The cells were incubated for 1 h at 37 °C in a 1:10 (v/v) dilution of Prestoblue reagent and α-MEM. After incubation, 2 × 100 μL of the medium from each well was collected into a black-walled 96-well plate. Prestoblue medium solution without cells was used as a blank sample. The fluorescence intensity associated with the metabolic activity of the cells was measured using a Wallac Victor^3 multilabel reader (PerkinElmer, Waltham, MA, USA) at an excitation of 544 nm and emission wavelength of 615 nm. The metabolic activity of the cells was analysed using seven independent sample replicates per time point.

2.2.6. Statistical analysis

All the numerical data were reported as the mean value and standard deviation (SD). The statistical testing of the cell proliferation results was performed with a two-way ANOVA using GraphPad Prism v8.4.3.

3. Results

3.1. Nanoparticle characterisation

BTNPs with and without coatings were characterised using STEM, and representative pictures are shown in Fig. 1A. The majority of the particles had a diameter of 50–80 nm (Fig. 1B–D). Most of the nanoparticles had a round morphology, while some oval and angular-shaped nanoparticles were also observed. The EDS analysis confirmed that these nanoparticles contained mainly barium, titanium, and oxygen, as expected. For the coated nanoparticles, aluminium and silicon were detected at ~1–2 wt%.

3.2. Scaffold characterisation

The porous 3D scaffolds were produced using the breath figure method by solvent casting the polymer solution under high humidity. Representative FE-SEM images showing the structure and size distribution of the pores are shown in Fig. 2. It was observed that the incorporation of the nanoparticles into the PLDLA scaffold influenced the pore formation and increased the pore size compared to the pure PLDLA scaffold. However, the SiO_2 coating disrupted the pore formation and did not form a honeycomb structure. The average pore size for the pure PLDLA scaffold was 1.6 μm (SD 0.3 μm), while it was 16.2 μm (SD 3.0 μm), 5.0 μm (SD 0.9 μm), and 3.2 μm (SD 1.3 μm) for the PLDLA/BTNP, PLDLA/BTNP-Al_2O_3 and PLDLA/BTNP-SiO_2 scaffolds, respectively. Consequently, the most suitable pore structure for cell migration into the scaffold was achieved using uncoated BTNPs. These 3D composite scaffolds had a pore diameter of approximately 16 μm and were the only ones with sufficiently large pores to allow cellular penetration. Therefore, the PLDLA/BTNP scaffold was chosen for further testing of

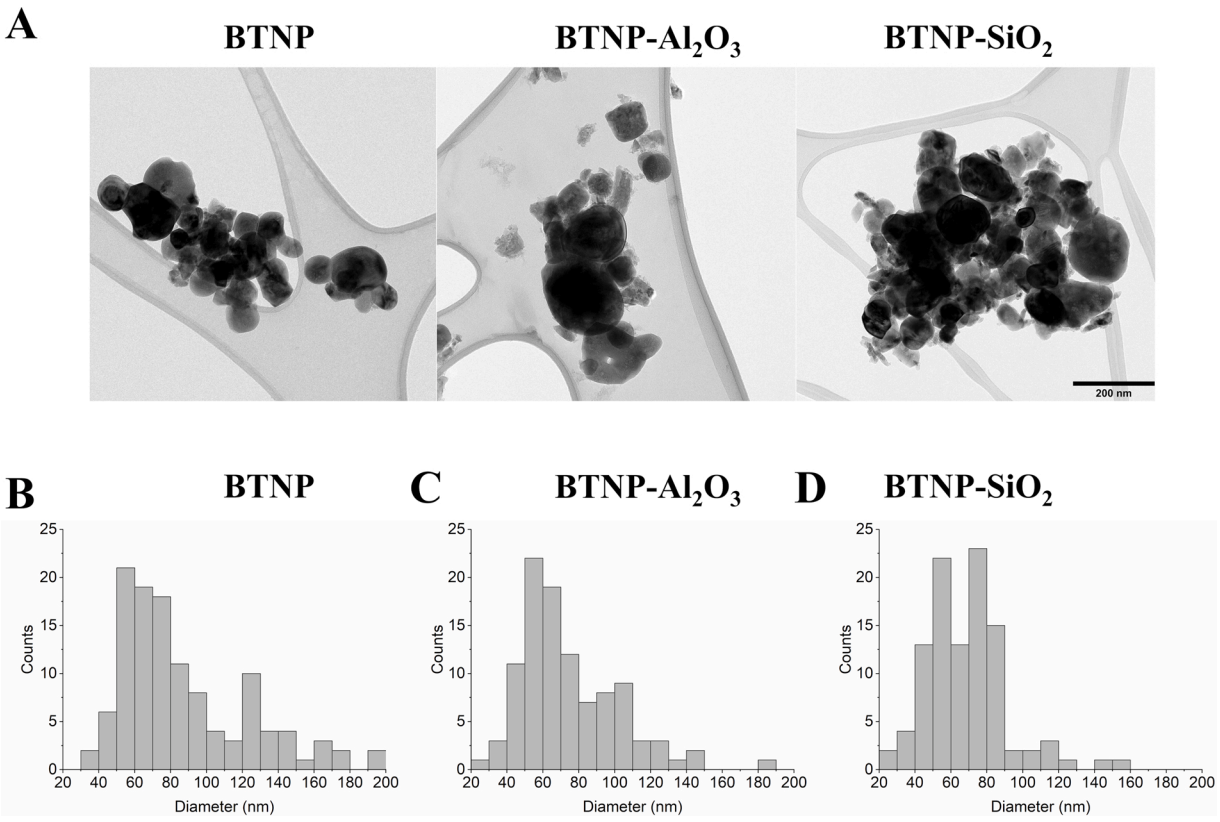

Fig. 1. Characterisation of barium titanate nanoparticles. A. Representative STEM images of barium titanate nanoparticles. Scale bar 200 nm. Diameter distribution of nanoparticles for **B.** uncoated BTNPs, **C.** Al_2O_3-coated BTNPs and **D.** SiO_2-coated BTNPs.
Abbreviations: STEM scanning transmission electron microscope; BTNP uncoated barium titanate nanoparticle; BTNP-Al_2O_3aluminium oxide coated barium titanate nanoparticle; BTNP-SiO_2 silicon dioxide coated barium titanate nanoparticle.

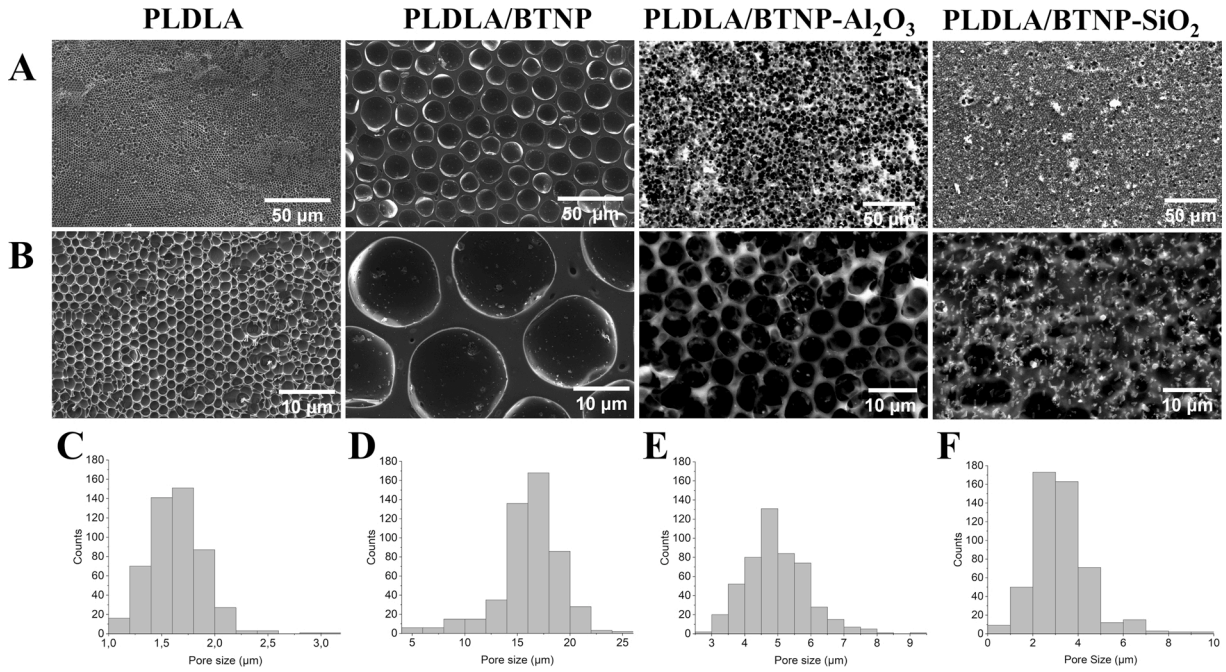

Fig. 2. Characterisation of scaffolds. Representative FE-SEM images of the scaffolds with **A.**scale bar 50 µm and **B.** scale bar 10 µm. The diameter distribution of pore size and average dimeter of the pores for **C.** PLDLA was 1.6 µm, **D.** for PLDLA/BTNP 16.2 µm, **E.** for PLDLA/BTNP-Al_2O_3 5.0 µm and **F.** for PLDLA/BTNP-SiO_2 3.2 µm.

Abbreviations: FE-SEM, field emission scanning electron microscope; PLDLA, poly-L/D-lactide copolymer; BTNP, barium titanate nanoparticle; PLDLA/BTNP, PLDLA and uncoated BTNP composite scaffold; PLDLA/BTNP-Al_2O_3, PLDLA and aluminium oxide coated BTNP composite scaffold; PLDLA/BTNP-SiO_2, PLDLA and silicon dioxide coated BTNP composite scaffold.

biocompatibility, and a pure PLDLA scaffold was kept as a control scaffold. The distribution of nanoparticles was studied with FE-SEM using backscattered electrons, where the BTNPs were seen as bright particles (Fig. 3). It was observed that the BTNPs were evenly distributed in the scaffold as small aggregates.

3.3. Biocompatibility of scaffolds

The biocompatibility of the PLDLA and PLDLA/BTNP scaffolds was investigated by culturing ovine stromal stem cells for two weeks. The morphology and cell attachment were evaluated using FE-SEM (Fig. 4), which confirmed that the cells were spread widely in both scaffolds. The increased pore size in the PLDLA/BTNP scaffolds provided a suitable porous structure for the cells to migrate into the 3D scaffold. Inside these pores, the cells maintained their round morphology, while on the surface of the scaffold they were elongated. Cells were connected to each other with thin filaments in the PLDLA/BTNP scaffold, while in the PLDLA they were spread into a wider area.

The cell viability was studied using the LIVE/DEAD assay, where green and red fluorescence emissions from calcein-AM and ethidium homodimer were used to indicate viable and dead cells, respectively. As shown in Fig. 5A, the cells remained alive for two weeks in both the PLDLA and PLDLA/BTNP scaffolds, indicating the biocompatibility of these scaffolds. On the PLDLA scaffolds, the cells spread on the surface,

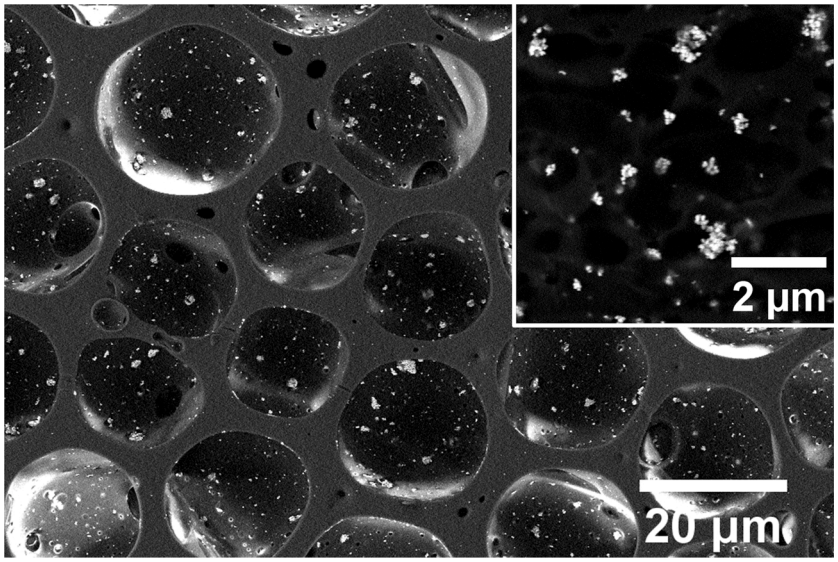

Fig. 3. Characterisation of composite scaffold. Representative FE-SEM image from PLDLA/BTNP composite scaffold using backscatter imaging, scale bars 20 µm and 2 µm.

Abbreviations: FE-SEM, field emission scanning electron microscope; PLDLA/BTNP, poly-L/D-lactide copolymer and uncoated barium titanate nanoparticle composite scaffold.

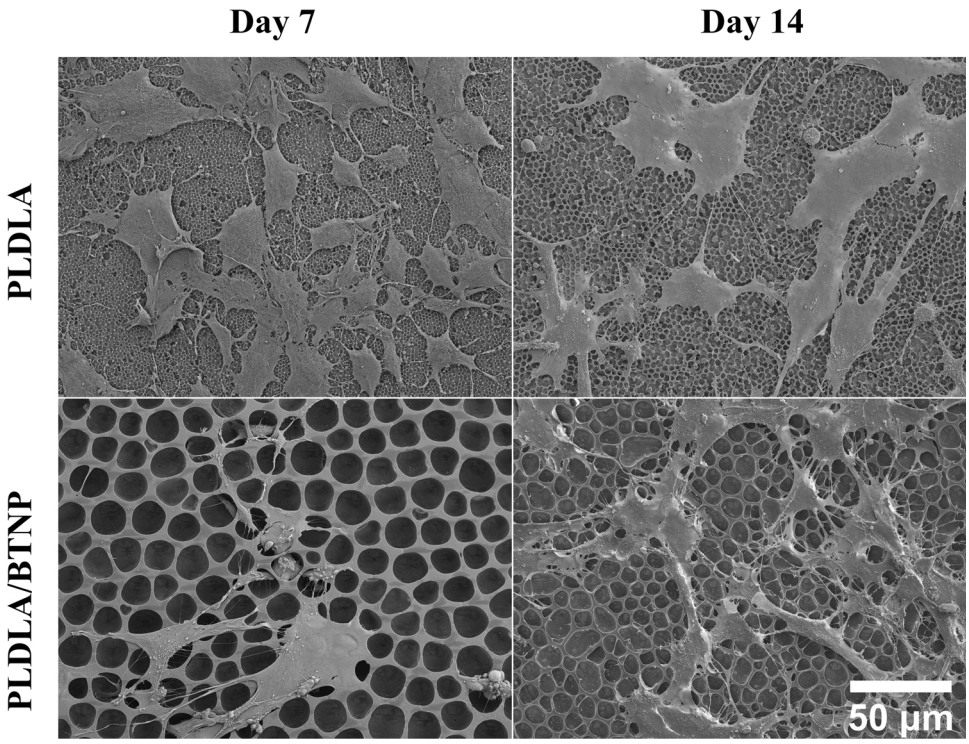

Fig. 4. Cell morphology and attachment to the scaffolds. Representative FE-SEM images after 7 and 14 days of culturing of ovine stromal stem cells on the scaffolds. Scale bar 50 µm.
Abbreviations: FE-SEM, field emission scanning electron microscope; PLDLA, poly-L/D-lactide copolymer; PLDLA/BTNP, PLDLA and uncoated barium titanate nanoparticle composite scaffold.

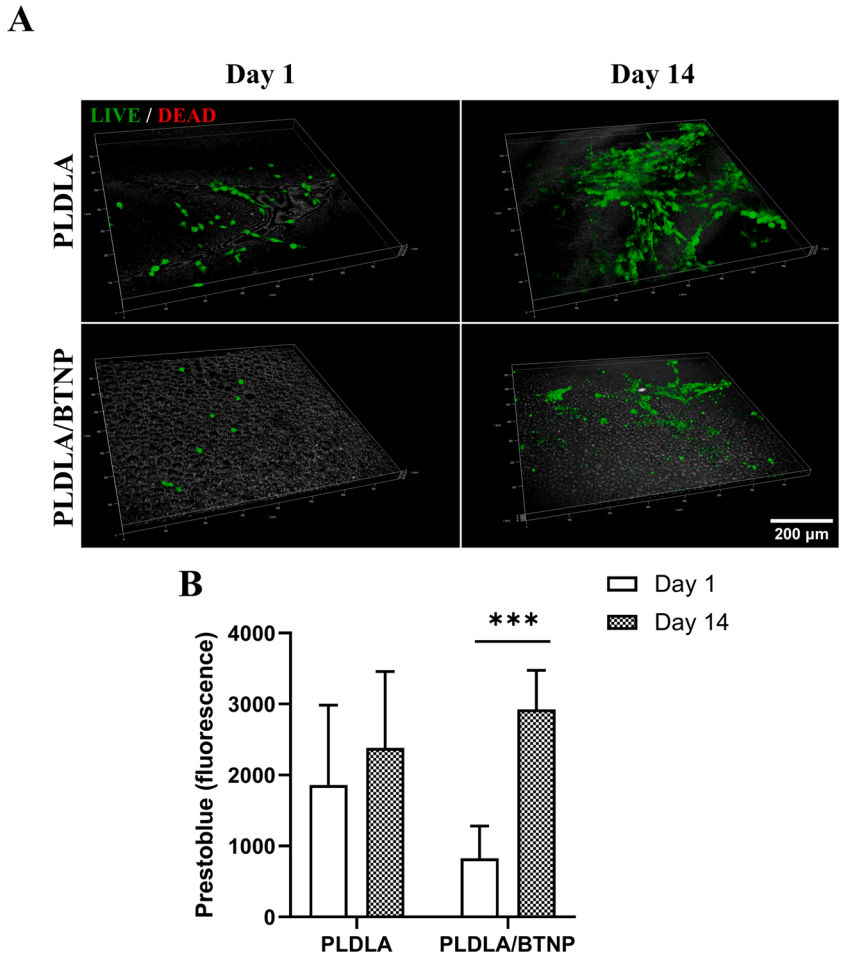

Fig. 5. The viability and metabolic activity of ovine stromal stem cells in the scaffolds. A. Cell viability at day 1 and 14 measured with LIVE/DEAD staining in PLDLA and PLDLA/BTNP scaffolds, live cells are shown in green and dead in red. Scale bar 200 µm **B.** Metabolic activity of the cells increased from day 1 to 14 according Prestoblue assay, $n = 7$, *** denotes statistical significance at $p < 0.001$.
Abbreviations: PLDLA, poly-L/D-lactide copolymer, PLDLA/BTNP, PLDLA and uncoated barium titanate nanoparticle composite scaffold.

whereas in the PLDLA/BTNP scaffolds, the cells permeated inside the pores and remained round.

Cell proliferation was measured with the Prestoblue assay, which showed increased metabolic activity in the scaffolds during two weeks of culturing (Fig. 5B). Prestoblue is a fluorometric resazurin-based assay, where the Prestoblue reagent is reduced by metabolically active cells. There was a significant increase in the cell metabolic activity between day 1 and day 14 in the PLDLA/BTNP scaffolds. On average, the increase in metabolic activity between time points was greater in the PLDLA/BTNP scaffolds than in the pure PLDLA scaffolds, indicating higher cell proliferation in the composite scaffold. Both the PLDLA and PLDLA/BTNP scaffolds were able to maintain cell viability and proliferation for 14 days in culture, indicating that the 3D scaffolds were biocompatible.

4. Discussion

This study demonstrated the successful utilisation of the breath figure method for incorporating BTNPs into porous PLDLA scaffolds. Different nanoparticles and their effects on the scaffold porosity were monitored while maintaining the same processing method and production conditions. BTNPs were chosen for this study because they are piezoelectric and could thus provide a means for the mechanical or electrical stimulation of cells. To the best of our knowledge, this is the first time that BTNPs have been incorporated into polymer scaffolds using the breath figure method. It was observed that the BTNPs affected the pore formation and increased the pore size. This was somewhat expected because it has previously been shown that silver nanoparticles (AgNPs) affect the pore formation in the breath figure method [30]. The incorporation of AgNPs into the PLA scaffold increased the regularity of the pore size and pore array. It was proposed that nanoparticles allow water droplets to spread wider on the polymer solution during the scaffold production process and thus create larger pores [30]. BTNPs tend to aggregate easily, making homogenous dispersions of BTNPs difficult to achieve. This is why different coatings are used to improve their dispersion in solutions and prevent the aggregation of particles [25]. Here, three different types of BTNPs (uncoated, Al_2O_3-coated, and SiO_2-coated) were studied to obtain a suitable scaffold structure. It was observed that uncoated BTNPs produced a pore size of 16.2 μm, while in the pure PLDLA scaffold it was 1.6 μm. Both the Al_2O_3-coated and SiO_2-coated BTNP composite scaffolds had pore sizes smaller than 5 μm. Thus, only uncoated BTNPs allowed water to condense to larger droplets during the production process, creating pores larger than cells. For this reason, uncoated BTNP scaffolds were chosen for biocompatibility testing because they provided the most suitable porous 3D structure for cell migration into the scaffold.

There have only been a few previous studies where BTNPs have been combined with polymer scaffolds and tested for biological applications [26,31]. Li et al. [26] used electrospinning to fabricate poly-(*L*-lactic acid) (PLLA) and BTNP composite scaffolds with BTNP contents of 1–10 wt%. BTNPs were surface-modified with sodium citrate and they had an average size of 100 nm. The incorporation of BTNPs into the scaffold improved the polygonal spreading and proliferation of mesenchymal stem cells [26]. Furthermore, Ciofani et al. [31] developed poly (lactic-co-glycolic) acid (PLGA) and BTNP composite scaffolds using the solvent casting method, where they used uncoated BTNPs with an average size of 200 nm. It was shown that 10 and 30 wt% mass fractions of BTNPs were suitable for culturing rat cardiomyocytes because enhanced cell proliferation and differentiation were observed [31]. A mass fraction of 20 wt% was selected for this study in order to obtain a high mass fraction of nanoparticles to optimise the incorporation process with the breath figure method, while simultaneously ensuring the biocompatibility of the scaffolds.

Stem cells, especially mesenchymal stem cells [32], are appropriate cell sources for tissue engineering because they can be collected from adults and have the potential to differentiate into other cell types such as osteocytes, chondrocytes, and adipocytes [33–37]. In this study, ovine bone marrow-derived stromal stem cells were used for biocompatibility testing. It was observed from the FE-SEM and LIVE/DEAD staining images that the ovine stromal stem cells remained inside the pores and maintained their spherical morphology in the PLDLA/BTNP scaffolds, where the pore size was larger than the size of the cells. In the pure PLDLA scaffolds, the pore size was smaller than the cell size, and thus cells spread on top of the scaffold. This result was in agreement with the literature indicating that in pores larger than mesenchymal stem cells, cells tend to migrate to the bottom of the pores and remain spherical, or while staying on top, cells stretch and attach to rims [13]. Conversely, in the pores smaller than cells, they have fewer surfaces to adhere to, leading to lower cell areas and a more polygonal cell shape. When the pore size is the same as the cell size, cells can spread more and elongate [12,38]. Regarding the tissue engineering of articular cartilage, the porous 3D structure of this study could provide a suitable microenvironment for chondrocytes to maintain their original morphology. This is important because it has been shown that scaffolds that can support a spherical morphology can increase the extracellular matrix production of chondrocytes [39,40]. Importantly, it has previously been shown that honeycomb structures can increase the ECM production of chondrocytes and sustain their spherical morphology [16].

According to the Prestoblue assay, a significant increase was observed in the cell metabolic activity in the PLDLA/BTNP scaffolds after 14 days of culturing. However, even though an increased cell amount could be detected in the LIVE/DEAD images, the PLDLA scaffolds had a slightly higher intensity of green on day 14. This could have been caused by different factors. First, some of the cells were inside the structure in the PLDLA/BTNP scaffolds, and the fluorescence signal was not able to easily penetrate through the material. This reduced the detected fluorescence intensity. Furthermore, the PLDLA/BTNP scaffolds maintained the round cell morphology by entrapping cells inside the pores. Thus, the cell area and detected fluorescence signal were smaller in the PLDLA/BTNP scaffolds.

Complex 3D scaffolds are needed in tissue engineering to restore the original function of damaged tissues [41,42]. Composite scaffolds can be used to improve the properties of regular scaffolds by incorporating multiple materials into one scaffold [22]. For instance, piezoelectric ceramics such as $BaTiO_3$ can enhance biological responses in implants [43]. Furthermore, it is known that the surface morphology and matrix stiffness affect stem cell behaviour and differentiation [12,44,45]. Therefore, additional studies on the BTNP concentration in a scaffold should be conducted to study the effect of the nanoparticles on the mechanical properties of the scaffold. In principle, BTNPs have the potential to tune tissue engineering applications into smart implants and provide electromechanical stimulation. The PLDLA/BTNP composite scaffolds produced in this study were found to be biocompatible, but further studies are planned to evaluate the effect of stimulated nanoparticles on cell behaviour.

5. Conclusion

In this study, the breath figure method was successfully applied to incorporate BTNPs into a PLDLA scaffold while maintaining a porous honeycomb-like structure. The use of uncoated BTNPs resulted in a composite scaffold with an optimal pore size for cell migration into the scaffold. Furthermore, the PLDLA/BTNP scaffolds were biocompatible and had an influence on the cell proliferation and morphology. To conclude, BTNP and PLDLA scaffolds provide promising composite structures for future tissue engineering applications.

Statement of significance

Piezoelectric scaffolds can provide electromechanical stimulation for cells, which makes them promising materials for future tissue engineering applications. Barium titanate nanoparticles (BTNPs) are non-toxic piezoelectric nanoparticles, and their potential in biological

applications has not been adequately utilised. Porosity is an important feature to obtain when developing a suitable scaffold structure for tissue repair. The breath figure method was used in this work to develop a porous 3D composite scaffold using BTNPs and a poly-L/D-lactide copolymer. Uncoated BTNPs increased the pore size of the scaffold and enabled cell migration into the pores. The created composite scaffold has great potential for use in future cartilage tissue engineering applications to preserve the natural phenotype of chondrocytes.

CRediT authorship contribution statement

H. Kemppi: Conceptualization, Methodology, Formal analysis, Investigation, Writing - original draft, Visualization. **M.A. Finnilä:** Conceptualization, Methodology, Writing - review & editing, Supervision. **G.S. Lorite:** Conceptualization, Methodology, Resources, Writing - review & editing. **M. Nelo:** Investigation, Writing - review & editing. **J. Juuti:** Resources, Writing - review & editing. **M. Kokki:** Resources, Writing - review & editing. **H. Kokki:** Resources, Writing - review & editing. **J. Räsänen:** Resources, Writing - review & editing. **A. Mobasheri:** Conceptualization, Writing - review & editing. **S. Saarakkala:** Conceptualization, Resources, Writing - review & editing, Supervision.

Declaration of Competing Interest

The authors report no declarations of interest.

Acknowledgements

This project was funded by the European Union's Horizon 2020 Research and Innovation programme under grant agreement No 814558 "RESTORE".

Author G. S. L. acknowledges the support of the Academy of Finland (decision no. 317437).

Author J. J. acknowledges the support of the Academy of Finland (decision no. 318203).

This work was carried out with the support of Biocenter Oulu, Light and Electron Microscopy Core Facilities, University of Oulu, Oulu, Finland, and the Centre for Material Analysis, University of Oulu, Oulu, Finland.

References

[1] R. Langer, J.P. Vacanti, Tissue engineering, Science (80-.) 260 (1993) 920–926, https://doi.org/10.1126/science.8493529.

[2] D. Howard, L.D. Buttery, K.M. Shakesheff, S.J. Roberts, Tissue engineering: strategies, stem cells and scaffolds, J. Anat. 213 (2008) 66–72, https://doi.org/10.1111/j.1469-7580.2008.00878.x.

[3] S.W. Crowder, V. Leonardo, T. Whittaker, P. Papathanasiou, M.M. Stevens, Material cues as potent regulators of epigenetics and stem cell function, Cell Stem Cell 18 (2016) 39–52, https://doi.org/10.1016/j.stem.2015.12.012.

[4] F. Guilak, D.M. Cohen, B.T. Estes, J.M. Gimble, W. Liedtke, C.S. Chen, Control of stem cell fate by physical interactions with the extracellular matrix, Cell Stem Cell 5 (2009) 17–26, https://doi.org/10.1016/j.stem.2009.06.016.

[5] F.J. O'Brien, Biomaterials & scaffolds for tissue engineering, Mater. Today 14 (2011) 88–95, https://doi.org/10.1016/S1369-7021(11)70058-X.

[6] T.W. Odom, J.C. Love, D.B. Wolfe, K.E. Paul, G.M. Whitesides, Improved pattern transfer in soft lithography using composite stamps, Langmuir 18 (2002) 5314–5320, https://doi.org/10.1021/la020169l.

[7] J.J. Norman, T.A. Desai, Methods for fabrication of nanoscale topography for tissue engineering scaffolds, Ann. Biomed. Eng. 34 (2006) 89–101, https://doi.org/10.1007/s10439-005-9005-4.

[8] M.J.P. Biggs, R.G. Richards, M.J. Dalby, Nanotopographical modification: a regulator of cellular function through focal adhesions, Nanomed. Nanotechnol. Biol. Med. 6 (2010) 619–633, https://doi.org/10.1016/j.nano.2010.01.009.

[9] M.T. Calejo, T. Ilmarinen, H. Skottman, M. Kellomäki, Breath figures in tissue engineering and drug delivery: state-of-the-art and future perspectives, Acta Biomater. 66 (2018) 44–66, https://doi.org/10.1016/j.actbio.2017.11.043.

[10] M.T. Calejo, J. Saari, H. Vuorenpää, E. Vuorimaa-Laukkanen, P. Kallio, K. Aalto-Setälä, S. Miettinen, H. Skottman, M. Kellomäki, K. Juuti-Uusitalo, Co-culture of human induced pluripotent stem cell-derived retinal pigment epithelial cells and endothelial cells on double collagen-coated honeycomb films, Acta Biomater. 101 (2020) 327–343, https://doi.org/10.1016/j.actbio.2019.11.002.

[11] H. Abe, Y. Hirai, H. Yabu, Thermally stable honeycomb-patterned porous films of a poly(L-lactic acid) and poly(D-lactic acid) stereo complex prepared using the breath figure technique, Macromol. Mater. Eng. 301 (2016) 523–529, https://doi.org/10.1002/mame.201500474.

[12] T. Kawano, M. Sato, H. Yabu, M. Shimomura, Honeycomb-shaped surface topography induces differentiation of human mesenchymal stem cells (hMSCs): uniform porous polymer scaffolds prepared by the breath figure technique, Biomater. Sci. 2 (2014) 52–56, https://doi.org/10.1039/c3bm60195a.

[13] Y. Liu, J. Xu, Y. Zhou, Z. Ye, W.S. Tan, Layer-by-layer assembled polyelectrolytes on honeycomb-like porous poly(ε-caprolactone) films modulate the spatial distribution of mesenchymal stem cells, Mater. Sci. Eng. C 78 (2017) 579–588, https://doi.org/10.1016/j.msec.2017.04.140.

[14] S. Foldberg, M. Petersen, P. Fojan, L. Gurevich, T. Fink, C.P. Pennisi, V. Zachar, Patterned poly(lactic acid) films support growth and spontaneous multilineage gene expression of adipose-derived stem cells, Colloids Surf. B Biointerfaces 93 (2012) 92–99, https://doi.org/10.1016/j.colsurfb.2011.12.018.

[15] M.A. Birch, M. Tanaka, G. Kirmizidis, S. Yamamoto, M. Shimomura, Microporous "Honeycomb" films support enhanced bone formation *in vitro*, Tissue Eng. Part A 19 (2013) 2087–2096, https://doi.org/10.1089/ten.tea.2012.0729.

[16] Y. Fukuhira, H. Kaneko, M. Yamaga, M. Tanaka, S. Yamamoto, M. Shimomura, Effect of honeycomb-patterned structure on chondrocyte behavior in vitro, Colloids Surfaces A Physicochem. Eng. Asp. 313–314 (2008) 520–525, https://doi.org/10.1016/j.colsurfa.2007.05.047.

[17] J.O. Eniwumide, M. Tanaka, N. Nagai, Y. Morita, J. de Bruijn, S. Yamamoto, S. Onodera, E. Kondo, K. Yasuda, M. Shimomura, The morphology and functions of articular chondrocytes on a honeycomb-patterned surface, Biomed Res. Int. (2014), https://doi.org/10.1155/2014/710354.

[18] M. Okamoto, B. John, Synthetic biopolymer nanocomposites for tissue engineering scaffolds, Prog. Polym. Sci. 38 (2013) 1487–1503, https://doi.org/10.1016/j.progpolymsci.2013.06.001.

[19] M.T. Calejo, T. Ilmarinen, H. Jongprasitkul, H. Skottman, M. Kellomäki, Honeycomb porous films as permeable scaffold materials for human embryonic stem cell-derived retinal pigment epithelium, J. Biomed. Mater. Res. - Part A. 104 (2016) 1646–1656, https://doi.org/10.1002/jbm.a.35690.

[20] Y. Fukuhira, E. Kitazono, T. Hayashi, H. Kaneko, M. Tanaka, M. Shimomura, Y. Sumi, Biodegradable honeycomb-patterned film composed of poly(lactic acid) and dioleoylphosphatidylethanolamine, Biomaterials 27 (2006) 1797–1802, https://doi.org/10.1016/j.biomaterials.2005.10.019.

[21] Y. Fukuhira, H. Yabu, K. Ijiro, M. Shimomura, Interfacial tension governs the formation of self-organized honeycomb-patterned polymer films, Soft Matter 5 (2009) 2037–2041, https://doi.org/10.1039/b821183c.

[22] G. Chen, T. Ushida, T. Tateishi, Scaffold design for tissue engineering, Macromol. Biosci. 2 (2002) 67–77, https://doi.org/10.1002/1616-5195(20020201)2:2<67::AID-MABI67>3.0.CO;2-F.

[23] G.G. Genchi, A. Marino, A. Rocca, V. Mattoli, G. Ciofani, Barium titanate nanoparticles: promising multitasking vectors in nanomedicine, Nanotechnology 27 (232001) (2016), https://doi.org/10.1088/0957-4484/27/23/232001.

[24] K. McNamara, S.A.M. Tofail, Nanoparticles in biomedical applications, Adv. Phys. X. 2 (2017) 54–88, https://doi.org/10.1080/23746149.2016.1254570.

[25] G. Ciofani, S. Danti, S. Moscato, L. Albertazzi, D. D'Alessandro, D. Dinucci, F. Chiellini, M. Petrini, A. Menciassi, Preparation of stable dispersion of barium titanate nanoparticles: potential applications in biomedicine, Colloids Surf. B Biointerfaces 76 (2010) 535–543, https://doi.org/10.1016/j.colsurfb.2009.12.015.

[26] Y. Li, X. Dai, Y. Bai, Y. Liu, Y. Wang, O. Liu, F. Yan, Z. Tang, X. Zhang, X. Deng, Electroactive BaTiO3 nanoparticle-functionalized fibrous scaffolds enhance osteogenic differentiation of mesenchymal stem cells, Int. J. Nanomed. 12 (2017) 4007–4018, https://doi.org/10.2147/IJN.S135605.

[27] G. Ciofani, S. Danti, D. D'Alessandro, L. Ricotti, S. Moscato, G. Bertoni, A. Falqui, S. Berrettini, M. Petrini, V. Mattoli, A. Menciassi, Enhancement of neurite outgrowth in neuronal-like cells following boron nitride nanotube-mediated stimulation, ACS Nano 4 (2010) 6267–6277, https://doi.org/10.1021/nn101985a.

[28] Finnish Goverment, Decree on the Protection of Animals Used for Scientific or Educational Purposes (564/2013), 2013 (n.d.). https://www.finlex.fi/fi/laki/kaannokset/2013/en20130564.pdf (Accessed August 26, 2020).

[29] The European Parliament and the Council of the European Union, Directive 2010/63/EU of the European Parliament and of the Council on the Protection of Animals Used for Scientific Purposes, 2010 (Accessed August 26, 2020), https://eur-lex.europa.eu/LexUriServ/LexUriServ.do?uri=OJ:L:2010:276:0033:0079:en:PDF.

[30] X. Jiang, X. Zhou, Y. Zhang, T. Zhang, Z. Guo, N. Gu, Interfacial effects of in situ-synthesized ag nanoparticles on breath figures, Langmuir 26 (2010) 2477–2483, https://doi.org/10.1021/la9027139.

[31] G. Ciofani, L. Ricotti, V. Mattoli, Preparation, characterization and in vitro testing of poly(lactic-co-glycolic) acid/barium titanate nanoparticle composites for enhanced cellular proliferation, Biomed. Microdevices 13 (2011) 255–266, https://doi.org/10.1007/s10544-010-9490-6.

[32] S.M. Richardson, J.A. Hoyland, R. Mobasheri, C. Csaki, M. Shakibaei, A. Mobasheri, Mesenchymal stem cells in regenerative medicine: opportunities and challenges for articular cartilage and intervertebral disc tissue engineering, J. Cell. Physiol. 222 (2010) 23–32, https://doi.org/10.1002/jcp.21915.

[33] R.J. Deans, A.B. Moseley, Mesenchymal stem cells: biology and potential clinical uses, Exp. Hematol. 28 (2000) 875–884, https://doi.org/10.1016/S0301-472X(00)00482-3.

[34] R. Mohammadinejad, M. Ashrafizadeh, A. Pardakhty, I. Uzieliene, J. Denkovskij, E. Bernotiene, L. Janssen, G.S. Lorite, S. Saarakkala, A. Mobasheri, Nanotechnological strategies for osteoarthritis diagnosis, monitoring, clinical

management, and regenerative medicine: recent advances and future opportunities, Curr. Rheumatol. Rep. 22 (2020), https://doi.org/10.1007/s11926-020-0884-z.
[35] C.R. Fellows, C. Matta, R. Zakany, I.M. Khan, A. Mobasheri, Adipose, bone marrow and synovial joint-derived mesenchymal stem cells for cartilage repair, Front. Genet. 7 (2016), https://doi.org/10.3389/fgene.2016.00213.
[36] J. Kobolak, A. Dinnyes, A. Memic, A. Khademhosseini, A. Mobasheri, Mesenchymal stem cells: identification, phenotypic characterization, biological properties and potential for regenerative medicine through biomaterial micro-engineering of their niche, Methods 99 (2016) 62–68, https://doi.org/10.1016/j.ymeth.2015.09.016.
[37] S.M. Richardson, G. Kalamegam, P.N. Pushparaj, C. Matta, A. Memic, A. Khademhosseini, R. Mobasheri, F.L. Poletti, J.A. Hoyland, A. Mobasheri, Mesenchymal stem cells in regenerative medicine: focus on articular cartilage and intervertebral disc regeneration, Methods 99 (2016) 69–80, https://doi.org/10.1016/j.ymeth.2015.09.015.
[38] T. Kawano, N. Iwama, H. Ishihata, H. Shimauchi, M. Shimomura, Preparation and biomedical application of self-organized honeycomb-patterned polymer films. Interface Oral Heal. Sci., Springer, Japan, 2011, pp. 22–26, https://doi.org/10.1007/978-4-431-54070-0_4, 2011.
[39] M. Russlies, P. Behrens, L. Wünsch, J. Gille, E.M. Ehlers, A cell-seeded biocomposite for cartilage repair, Ann. Anat. 184 (2002) 317–323, https://doi.org/10.1016/S0940-9602(02)80045-0.
[40] R. Izquierdo, N. Garcia-Giralt, M.T. Rodriguez, E. Cáceres, S.J. García, J.L. Gómez Ribelles, M. Monleón, J.C. Monllau, J. Suay, Biodegradable PCL scaffolds with an interconnected spherical pore network for tissue engineering, J. Biomed. Mater. Res. Part B Appl. Biomater. 85A (2008) 25–35, https://doi.org/10.1002/jbm.a.31396.
[41] M.J. Webber, O.F. Khan, S.A. Sydlik, B.C. Tang, R. Langer, A perspective on the clinical translation of scaffolds for tissue engineering, Ann. Biomed. Eng. 43 (2015) 641–656, https://doi.org/10.1007/s10439-014-1104-7.
[42] E.S. Place, N.D. Evans, M.M. Stevens, Complexity in biomaterials for tissue engineering, Nat. Mater. 8 (2009) 457–470, https://doi.org/10.1038/nmat2441.
[43] F.R. Baxter, C.R. Bowen, I.G. Turner, A.C.E. Dent, Electrically active bioceramics: a review of interfacial responses, Ann. Biomed. Eng. 38 (2010) 2079–2092, https://doi.org/10.1007/s10439-010-9977-6.
[44] A.J. Engler, S. Sen, H.L. Sweeney, D.E. Discher, Matrix elasticity directs stem cell lineage specification, Cell 126 (2006) 677–689, https://doi.org/10.1016/j.cell.2006.06.044.
[45] L. Krishna, K. Dhamodaran, C. Jayadev, K. Chatterjee, R. Shetty, S.S. Khora, D. Das, Nanostructured scaffold as a determinant of stem cell fate, Stem Cell Res. Ther. 7 (2016) 1–12, https://doi.org/10.1186/s13287-016-0440-y.